JACS
JOURNAL OF THE AMERICAN CHEMICAL SOCIETY
Article
pubs.acs.org/JACS

Copper Benzene Tricarboxylate Metal–Organic Framework with Wide Permanent Mesopores Stabilized by Keggin Polyoxometallate Ions

Lik H. Wee,[†] Christian Wiktor,[‡] Stuart Turner,[‡] Willem Vanderlinden,[§] Nikki Janssens,[†] Sneha R. Bajpe,[†] Kristof Houthoofd,[†] Gustaaf Van Tendeloo,[‡] Steven De Feyter,[§] Christine E. A. Kirschhock,*[,†] and Johan A. Martens[†]

[†]Centre for Surface Chemistry and Catalysis, KU Leuven, Kasteelpark Arenberg 23, B-3001, Leuven, Belgium

[‡]EMAT, University of Antwerp, Groenenborgerlaan 171, B-2020, Antwerp, Belgium

[§]Molecular and Nanomaterials, Laboratory of Photochemistry and Spectroscopy, KU Leuven, Celestijnenlaan 200f, B-3001, Leuven, Belgium

Supporting Information

ABSTRACT: Porous solids with organized multiple porosity are of scientific and technological importance for broadening the application range from traditional areas of catalysis and adsorption/separation to drug release and biomedical imaging. Synthesis of crystalline porous materials offering a network of uniform micro- and mesopores remains a major scientific challenge. One strategy is based on variation of synthesis parameters of microporous networks, such as, for example, zeolites or metal–organic frameworks (MOFs). Here, we show the rational development of an hierarchical variant of the microporous cubic $Cu_3(BTC)_2$ (BTC = 1,3,5-benzenetricarboxylate) HKUST-1 MOF having strictly repetitive 5 nm wide mesopores separated by uniform microporous walls in a single crystal structure. This new material coined COK-15 (COK = Centrum voor Oppervlaktechemie en Katalyse) was synthesized via a dual-templating approach. Stability was enhanced by Keggin type phosphotungstate (HPW) systematically occluded in the cavities constituting the walls between the mesopores.

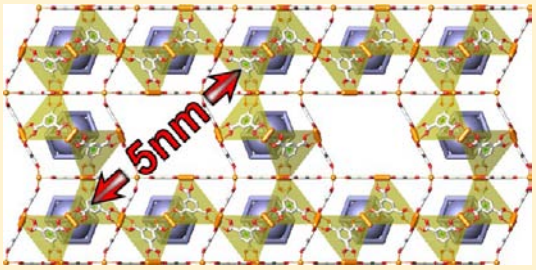

INTRODUCTION

Metal–organic frameworks (MOFs) are a relatively new class of materials obtained by connecting metal ions with organic linkers through coordinative bonding.[1] A large variety of MOFs have already been obtained by variation of metal and linker, and using combinations. The availability of such a wealth of primary building units offers an unprecedented toolbox for creating porosity and chemical functionality.[2−4] The large majority of reported MOFs have micropores (pores with diameter of less than 2 nm according to International Union of Pure and Applied Chemistry (IUPAC)).[5−9] MOFs with mesopores would open up additional application fields, for example, drug delivery and bioimaging,[10,11] gene therapy, functional peptidomics,[12] and enzymatic catalysis.[13] Extending the linkers is an obvious way to obtain mesoporous (pore size = 2−50 nm) MOFs.[9,14−21] However, this concept is limited, as with increasing linker size, the framework rigidity tends to decrease or the system starts to manifest interpenetrating frameworks.[22,23] Hierarchical MOFs with mesopores introduced into a microporous parent material are a further option. The mesopores across the microporous matrix are expected to facilitate molecular transport and thus to improve efficiency of catalytic and adsorptive processes, similar to inorganic hierarchical materials.[24,25] Accordingly, surfactant-templated routes to introduce mesoporosity in microporous MOFs have been reported.[26−28] Up to now, these efforts resulted in MOFs with worm-holes, lacking discernible long-range ordering.[26,27] Furthermore, mesoporous MOF materials often collapse after surfactant removal.[28] Here, we report room temperature synthesis of a new robust MOF material with strictly repetitive 5 nm wide mesopores separated by uniform microporous walls in a single crystal synthesized via a dual-templating approach involving Keggin type phosphotungstate (HPW) and cetyltrimethylammonium bromide (CTAB) as structure directing agents. The MOF framework is stabilized by HPW systematically occluded in the cavities constituting the walls between the mesopores. The new mesoporous MOF is coined COK-15, with idealized formula $(CTA)_1[Cu_{46}(C_9H_3O_6)_{24}(OH)_{12}](PW_{12}O_{40})_3{\cdot}xH_2O$. COK-15 is highly crystalline with a monoclinic structure and systematic mesopores corresponding to the [110] crystallographic direction of a hexagonal variant of the cubic $Cu_3(BTC)_2$ HKUST-1.

HKUST-1 $Cu_3(BTC)_2$ is a microporous MOF with three-dimensional cubic network wherein Cu(II) dimers are linked

Received: March 8, 2012
Published: June 6, 2012

dx.doi.org/10.1021/ja302089w | J. Am. Chem. Soc. 2012, 134, 10911−10919

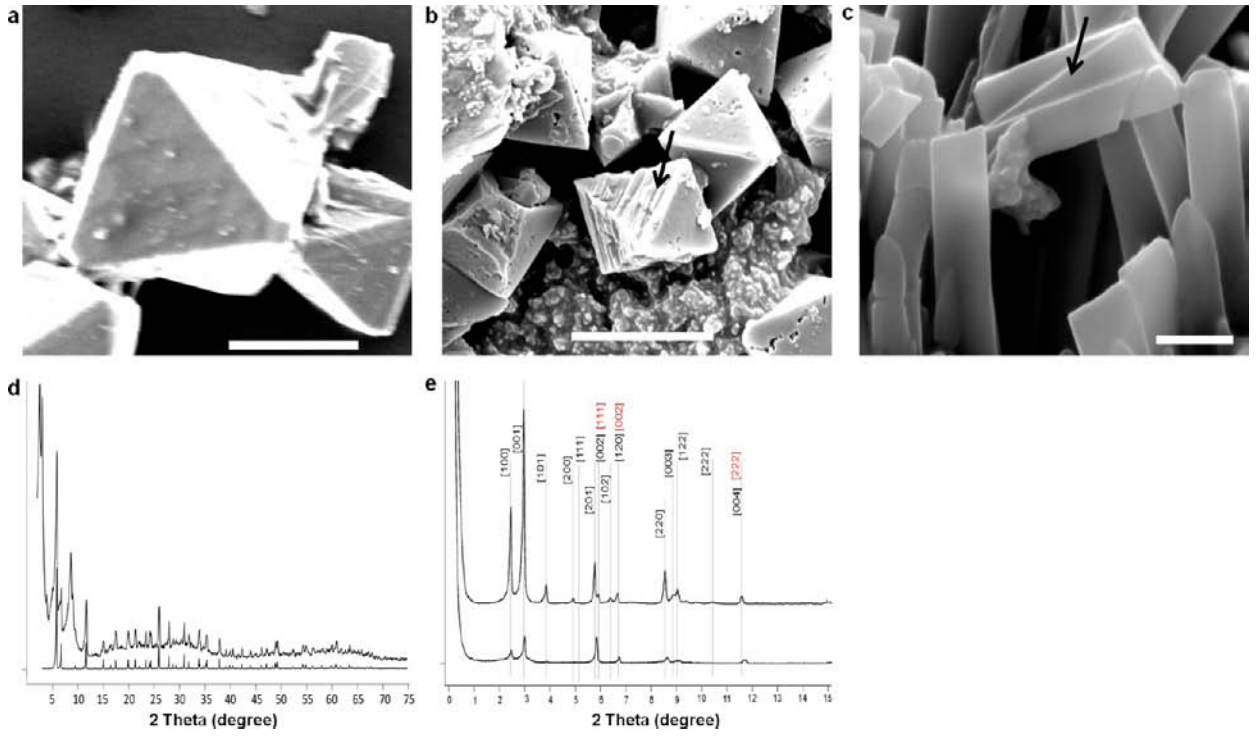

Figure 1. SEM investigation of the formation of COK-15. (a) Microporous HKUST-1 HPW@$Cu_3(BTC)_2$ with typical octahedral morphology. Scale bar: 20 μm. (b) COK-15a. Octahedral crystals with holes in their faces dominate the morphology. Some octahedra appear significantly twinned along [111]. The arrow in (b) shows such a distortion. Next to the crystals, a grainy phase is observed. Scale bar: 5 μm. (c) Slab-like lamellar morphology of COK-15. Almost no octahedral crystals are observed. Scale bar: 1 μm. SEM images show a distinct change in morphology from typical octahedral to lamellar slab-like crystals. (d and e) XRD patterns of COK-15: (d) XRD patterns of COK-15 (top) compared to microporous HKUST-1 HPW@$Cu_3(BTC)_2$ (bottom). (e) Comparison of XRD patterns between lamellar phase of COK-15 (top) and COK-15a (bottom) in the low angle region and indexation of the low angle region of the material. In black: *P6* space group with $a = b = 4.1$ nm and $c = 3.1$ nm. In red: indices according to the cubic space group $Fm\bar{3}m$ of the parent structure.

into paddlewheels by BTC. This MOF, first reported by Chui et al.,[5] is now one of the most studied MOFs. The pore structure of HKUST-1 consists of small octahedral cages connected to form two types of large cavities of cubooctahedral symmetry. One of these large cages is ideally suited for encapsulation of polyoxometalates (POMs) added to the hydrothermal synthesis.[29,30] Several MOFs bearing POMs have been reported and shown to be effective in catalysis.[14,31−37] In most cases, the POM is added to the hydrothermal synthesis and found in the cavities afterward. In the case of the HKUST-1, however, it was discovered strong interaction between Cu(II) and Keggin type HPW ions leads to spontaneous self-assembly of microporous HKUST-1 HPW@$Cu_3(BTC)_2$ (Supporting Information Figure S1) at room temperature.[38] The Keggin ion acts as a templating species during synthesis and stabilizes the microporous structure via the synergism between metal and Keggin ions.[39−41] In this case, the MOF assembly results in strictly systematic encapsulation of POM molecules. The mild conditions and strong template action of POM prompted the attempt to organize the crystal assembly on the next higher level, aiming to introduce organized mesopores in the structure. Mesoporosity can be generated by surfactants via a liquid-crystal template mechanism as known from mesoporous silicate materials such as MCM-41,[42] SBA-15,[43] and COK-12.[44] The present synthesis was based on the concept that the Keggin ions serve as molecular template for the structural motif of the MOF, while cetyltrimethylammonium bromide (CTAB) directs these units in an ordered mesoporous structure.

EXPERIMENTAL SECTION

Synthesis of COK-15. COK-15 materials were prepared from a synthesis mixture containing a molar composition of 18 Cu/10 BTC/HPW/CTAB/170 EtOH/2000 H_2O. In a typical synthesis, 1.45 g of copper(II) nitrate trihydrate ($Cu(NO_3)_2{\cdot}3H_2O$) (99−104%, Sigma-Aldrich) and 0.96 g of phosphotungstic acid hydrate ($H_3PW_{12}O_{40}{\cdot}nH_2O$) (for microscopy, Fluka) were dissolved in 12 mL of distilled water. Another solution containing 0.70 g of BTC (98%, Acros) and 0.12 g of CTAB (99+%, Acros) dissolved in 16 mL of absolute ethanol (BDH) was prepared. Both solutions were combined and mixed under vigorous stirring for approximately 30 min and were aged without stirring for a further 5 days at room temperature. The solid product was washed with water by filtration and dried in an air oven at 60 °C for 24 h. To remove CTAB, Soxhlet extraction with ethanol (laboratory use, Chem-Lab) was performed for 48 h. The product was dried in air at 60 °C. Alternatively, CTAB leaching was also performed using 0.25 mL of acetic acid (99−100%, Chem-Lab) or formic acid (99−100%, Chem Lab) in 250 mL of ethanol under reflux at 77 °C for 1 h, followed by filtration, washing with water/ethanol (50:50 (v/v) mixture and drying at 60 °C. The leaching was repeated with 0.125 mL of acetic acid.

Reference HKUST-1 HPW@$Cu_3(BTC)_2$ was prepared according to ref 30. A total of 1.215 g of $Cu(NO_3)_2{\cdot}3H_2O$ and 0.8 g of $H_3PW_{12}O_{40}{\cdot}nH_2O$ were dissolved in 10 mL of distilled water. Then, 0.5825 g of BTC was dissolved in 14 mL of absolute ethanol. The two solutions were mixed under vigorous stirring for 5 min and hydrothermally treated in a Teflon-lined autoclave at 110 °C for 16 h. The solid product was washed with distilled water and dried. Reference HKUST-1 $Cu_3(BTC)_2$ was synthesized according to ref 5. A total of 0.435 g of $Cu(NO_3)_2{\cdot}3H_2O$ was dissolved in 6 mL of distilled water and mixed with 6 mL of ethanolic solution containing 0.21 g of dissolved

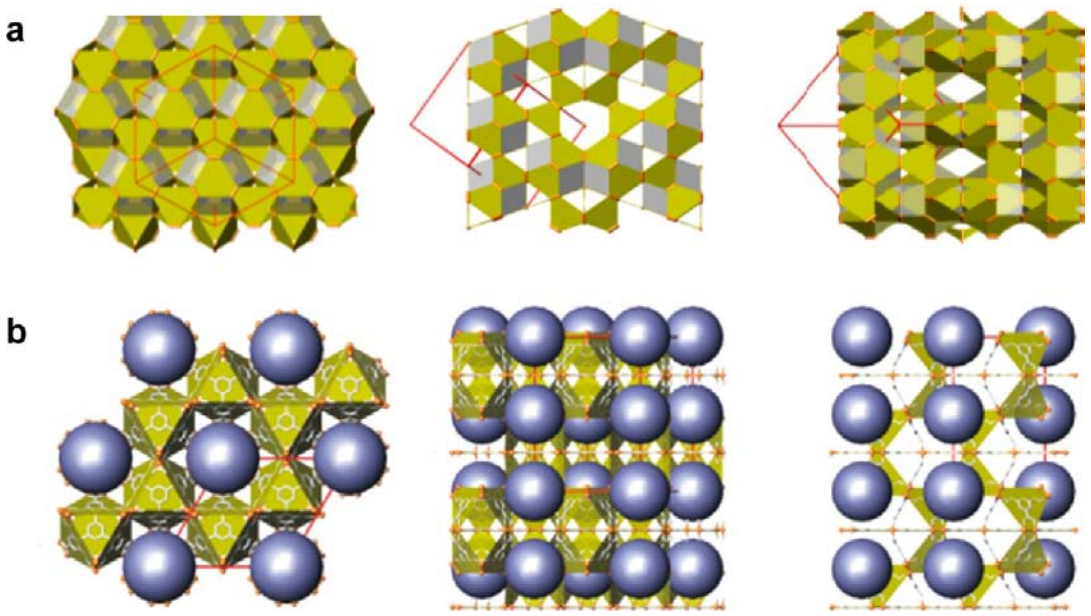

Figure 2. Building principle of COK-15 based on twinning. (a) Twinning of the cubic parent structure along [111] might explain the observed distortion of the octahedra observed by SEM and the hexagonal symmetry assigned to the diffraction pattern. Cages filled with HPW are shown as gray polyhedra. From left to right: view along [111], [110], and [11$\bar{2}$] of the cubic unit cell (shown in red). (b) Structures assembled by (a) ST at cubic (111) planes. From left to right, views along [001], [120], and [100].

BTC. The crystallization was performed at 180 °C for 12 h. The solid was washed with water/ethanol mixture and dried at 60 °C.

Characterization. Bright-field transmission electron microscopy (TEM) and electron diffractions experiments were carried out on a Philips CM20 microscope operated at 200 kV acceleration voltage. High-angle annular dark field−scanning transmission electron microscopy (HAADF-STEM) images were acquired on a Tecnai G2 microscope operated at 200 kV, with a convergence semiangle α of 10 mrad and an acceptance semiangle β of 36 mrad. Electron diffraction pattern simulations were performed using the Carine software package. All experiments were carried out at liquid nitrogen temperature using a GATAN cooling stage. Atomic force microscopy (AFM) analysis was performed using a nanoscope IV AFM (Multimode, Veeco), equipped with a 16 μm scanner (E-scanner) and soft silicon cantilevers (AC240TS, Olympus) operated in intermittent contact mode. A pellet of compressed COK-15 material was glued onto a metal support. By employing the microscope optical access, a selected crystal was positioned directly under the AFM tip. Scanning was performed with optimized feedback parameters and scan frequencies of 0.5−2 Hz, depending on the image size and topography. Images were analyzed using SPIP software (scanning probe image processor, v5.0.1, Image Metrology). Raw data were only plane-fitted before being subjected to further analysis. Low-angle X-ray diffraction analysis (XRD) was performed using a SAXSess mc^2 (Anton Paar GmbH, Graz, Austria) instrument. The sample was loaded into a vacuum-tight rotor cell and measured using line-collimated Cu Kα radiation and an image plate detector. Measurements were performed for 5 min at room temperature (25 °C). Diffraction patterns were normalized to incident beam intensity. Background subtraction and correction for instrumental broadening was performed using the SAXSquant software. The scattering of the empty rotor cell was subtracted as background. The morphology of COK-15 was investigated by scanning electron microscopy (SEM) on a Philips XL-30 FEG instrument equipped with a tungsten filament. Prior to analysis, samples were spread on carbon discs mounted to SEM aluminum pin stubs and gold sputtered. N_2 adsorption isotherms were collected from a N_2 adsorption instrument (Micromeritics Tristar 3000) at −196 °C. Before measurement, samples were degassed overnight at 110 °C under N_2 gas flow. The ^{31}P MAS NMR spectra were recorded on a Bruker AMX300 spectrometer (7.0 T), using the single-pulse excitation method. A total of 3503 scans were accumulated with a recycle delay of 20 s. The pulse length was 2.0 μs. The samples were packed in 4 mm Zirconia rotors, and the spinning frequency of the rotor was 6 kHz. A solution of 2 mL of orthophosphoric acid (85%, Normapur VWR) in 2 mL of water was used as chemical shift reference. Infrared spectra were recorded using a Nicolet 6700 FTIR spectrometer with DTGS detector (128 scans, 2 cm^{-1} resolution). The COK-15 sample was pressed into a self-supporting wafer (2 cm^2 area, 7 mg cm^{-2}), which was mounted in a cell with ZnSe windows. Before recording spectra, the sample was degassed in vacuum at 573 K.

Chemical Analysis. COK-15 (Soxhlet extracted) had an elemental composition (wt %, anhydrous) comprising 39.6% W, 16.2% Cu, 17.4% C, and 0.56% P. According to TGA (Supporting Information Figure S2), the water content estimated from the weight loss from 20 to 120 °C was ca. 4 wt %. The total weight loss in the temperature range 20−800 °C was ca. 30 wt %.

Catalytic Evaluation. Methanolysis of styrene oxide (97+%, Acros) with methanol (HPLC grade, BDH) was performed in close vials heated in a copper block at 40 °C and magnetically stirred at 1000 rpm. In a typical reaction, 1.25 mmol of styrene oxide was added to 7.5 mL of methanol. Then, 50 mg of solid catalyst (COK-15, microporous HKUST-1 HPW@$Cu_3(BTC)_2$, HKUST-1 $Cu_3(BTC)_2$, and zeolite HZSM-5 (Si/Al = 80, Süd-Chemie AG)) was tested. Aliquots of the reaction products were withdrawn with a microsyringe after 1, 2, 3, and 4 h of reaction and analyzed with GC (Chrompack 8760 WCOT fused silica capillary column, 30 m). Absence of leaching of catalytic elements from COK-15 was confirmed by the absence of further reaction after catalyst removal via centrifugation after 1 h reaction. Recycling tests were performed by charging new styrene oxide feed in a semicontinuous way every 3 h.

■ RESULTS AND DISCUSSION

Pure cubic microporous HKUST-1 material usually crystallizes in large octahedra (Figure 1a). In presence of low concentrations of CTAB (2 times lower than for COK-15 synthesis, denoted as COK-15a), octahedral crystals with (111) faces containing holes, visible even by SEM were observed. Some crystals appeared elongated in this direction, which could be achieved by extended twinning (Figure 1b, shown by an arrow). This could indicate the CTAB is prompting the material to deviate from the cubic

dx.doi.org/10.1021/ja302089w | J. Am. Chem. Soc. 2012, 134, 10911−10919

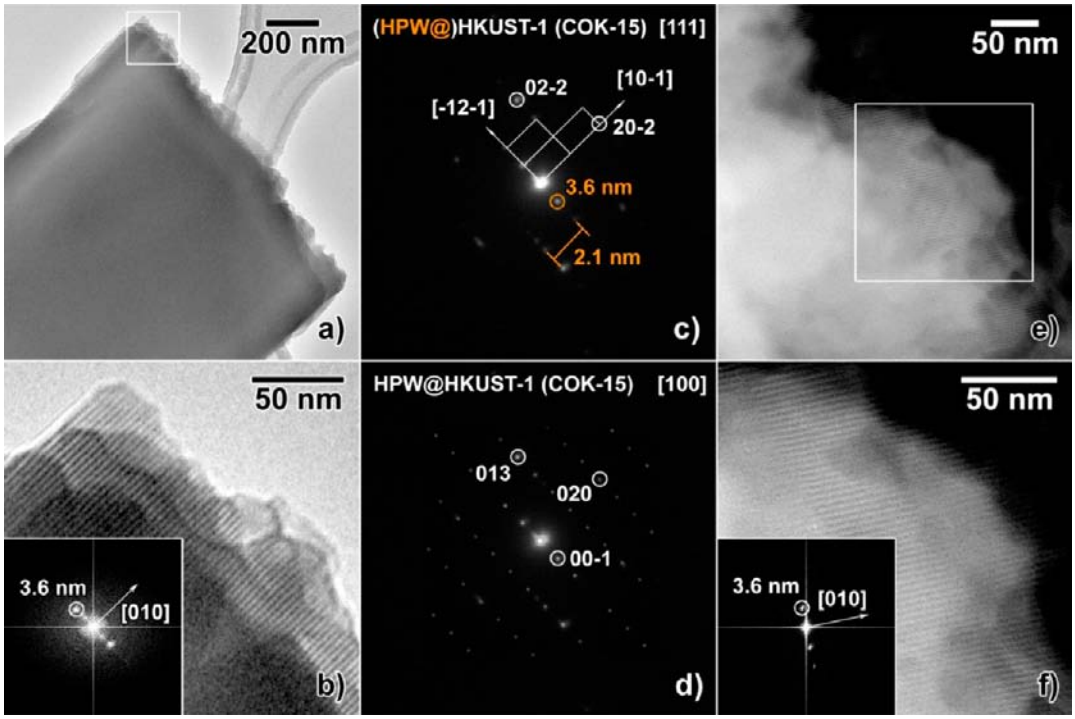

Figure 3. TEM analysis of COK-15 material. (a) Bright-field TEM image of a typical lamellar crystal. (b) Enlarged image of the region indicated in (a) showing the pore repetition. Inset: Fourier transform evidence a pore spacing of 3.6 nm. (c) Electron diffraction pattern of the COK-15 in (a), showing reflections related to HKUST-1 (in white) and reflections related to the mesoporous superstructure (in orange). (d) Simulated COK-15 diffraction pattern overlaid on the experimental diffraction pattern. (e) HAADF-STEM image of a similar crystal. (f) Enlarged image of the region indicated in (e). Inset: Fourier transform evidence a pore repetition of 3.6 nm.

toward a hexagonal symmetry. Next to the large crystals, another phase was observed which did not show marked faceting and appeared flaky to grainy. SEM images of COK-15 (Figure 1c), synthesized with higher amounts of CTAB, showed a new morphology: extended flat slabs were observed. The grainy phase, still present to some extent, appeared more flaky. Peculiarly, the crystals appeared terminated with rectangular faces which seemed to contradict the assumed hexagonal reconstruction of the original cubic structure. Despite the absence of the typical octahedra, the XRD powder pattern (Figure 1d) showed reflections typical for HKUST-1 or a hexagonal variant but also very well resolved reflections at low angles. Still, the XRD signals coinciding with a hexagonal symmetry persisted and increased in clarity in these samples.

The XRD pattern of COK-15 (Figure 1d) showed sharp reflections appearing at low angles ($<5°/2\theta$) suggesting a high degree of mesoscopic ordering. The wide-angle XRD diffractions were closely related to the microporous HKUST-1 HPW@$Cu_3(BTC)_2$. A closer investigation of the powder pattern (Figure 1e) at low angles revealed the sharp new reflections as well as the reflections usually assigned to HKUST-1 could indeed be tentatively assigned with a 3D hexagonal structure with lattice contants of $a = b = 4.1$ nm and c being a multiple of 1.5 nm, the typical distance of (111) planes in the cubic HKUST-1. Using this indexation, the [111] direction of the cubic parent phase coincides with the c direction of the twinned structure (Figure 1e). To understand the building scheme of the new material, at first the successful hexagonal indexation was used. The observation from XRD that the planar spacing of the (111) planes of the cubic parent material coincided with distances observed along a possible hexagonal axis of the new structure and the curious distortions of the octahedra seen in SEM led to the conclusion the mesoporous phase may consist of (111) planes of the cubic phase stacked in different ways. On the basis of the known structure of the cubic parent material, an attempt was made to assemble model structures to explain the experimental observations. For this, the structural relationship of the (111) plane in $Fm\bar{3}m$ (fcc) and the (001) plane in $P6_3/mmc$ (hcp) was exploited (Figure 2a). The most simple twinning of the basic fcc structure, twinning at every (111) plane, resulted in straight columns of cages connected via one triangular face. The unit cell of this single twin structure (ST model) had lattice constants of a = 2.1 nm and c = 3.1 nm in the hcp space group (Figure 2b). The simulated powder pattern of these structures showed rather good agreement with the observed data. However, reflections around 3 and 3.8° (2θ) were not reproduced and some simulated reflections at higher angles were not observed. For example, the rather strongly simulated [110] reflection was almost absent experimentally, whereas the measured [102] reflection could not be adequately reproduced. This indicated these model structures needed further improvement. Obviously, the structure of the crystalline COK-15 could not be solved exclusively by XRD, considering the large unit cell and the complex structure.[45] Especially the question how the mesopores are oriented with respect to the hexagonal axis could not conclusively be solved with XRD. Therefore, the materials were studied by TEM and AFM.

TEM analysis of MOF materials is challenging as, in many circumstances, MOFs are extremely sensitive to the electron beam and often collapse immediately upon irradiation.[46] However, the strong stabilization of the elemental building units of the $Cu_3(BTC)_2$ material by the encapsulated Keggin HPW ions was assumed to allow a crystallographic study of COK-15 by TEM. Also, the presence of the heavy HPW

dx.doi.org/10.1021/ja302089w | J. Am. Chem. Soc. 2012, 134, 10911−10919

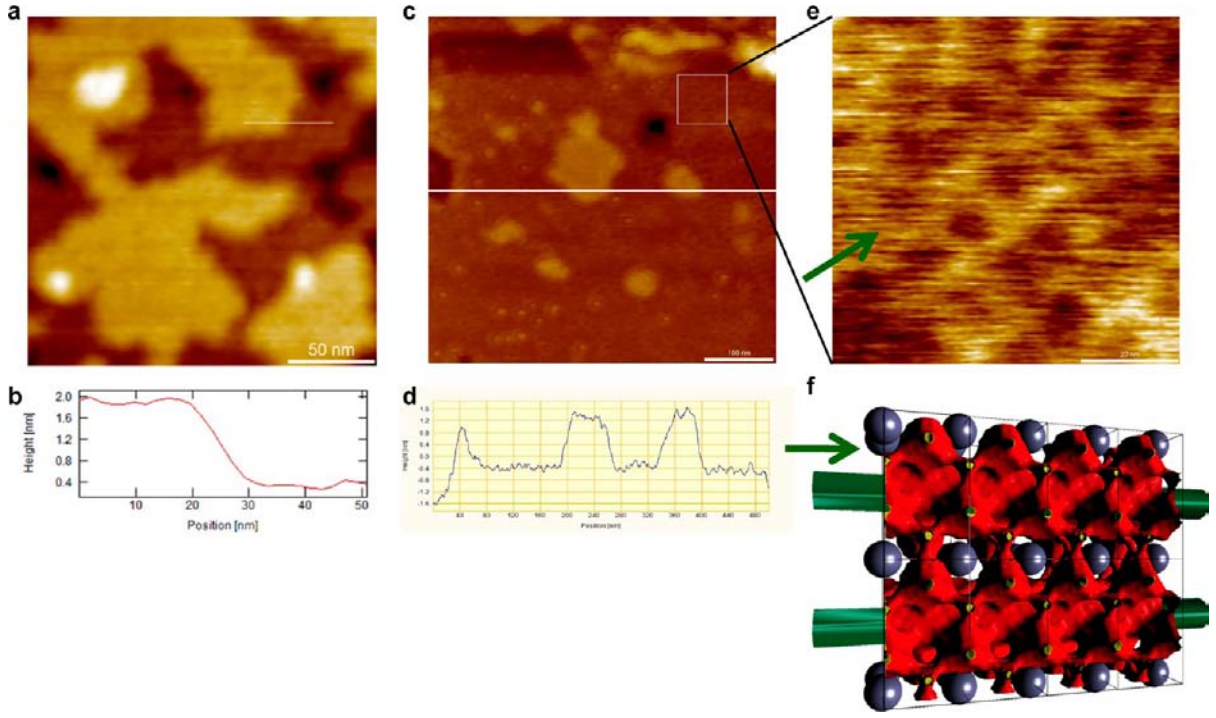

Figure 4. AFM analysis of COK-15. (a) Topography image of COK-15, (b) Cross-sectional analysis as marked in image (a) by white line. (c) AFM image of COK-15a taken in air using tapping mode and (d) the corresponding crosshair analysis along *x*-axis as marked in image (c) by white line. Consistent step heights of 1.5 nm were observed, which led to the identification of the slab surface as the original hexagonal layer. (e) Magnified AFM image of COK-15a. Closer inspection of the face led to observation of rectangular structures, consistent with the TEM images. (f) A surface of the final structure model (vide infra) corresponding to the view direction of TEM and AFM. Also here, rows of alternating height perpendicular and along to the pore direction (shown by green arrow) are observed. Keggin ions shown as blue spheres; red planes indicate the surface obtained by rolling a ball of 0.15 nm over the final model structure.

systematically occluded in the structure increased the contrast between microporous walls and mesopores during TEM analysis. To limit the risk of beam damage, as-synthesized COK-15 still containing CTAB was studied at liquid nitrogen temperature. These pictures (Figure 3) provided detailed information on the presence of highly ordered mesostructures in long-range ordering and their orientation with respect to the parent microporous structure. In Figure 3a,b, bright-field TEM images of a typical lamella are displayed. The highly ordered mesostructure of COK-15 is clearly visible, obviously due to the contrast between Keggin ions contained in microporous wall structures, next to the less dense mesopores. Figure 3b clearly shows alternating contrast in parallel lines with a distance of 3.6 nm. Similar parallel pores are visible in mass−thickness Z-contrast STEM images as shown in Figure 3e,f. In the direction perpendicular to the pore direction, diffraction (Figure 3c) revealed a lattice spacing of 2.1 nm. In comparison to the original cubic HKUST-1 HPW@$Cu_3(BTC)_2$ framework and the constructed hexagonal lattice ST, these reflections corresponded to (110)/(11$\bar{2}$) in the cubic and (110)/(120) in the hexagonal settings. Such an assembly was identified as a reduction of the hexagonal symmetry to an orthorhombic or monoclinic setting with lattice distances of 2.1 and 3.6 nm, in excellent agreement with lattice spacings in the ST model. However, the third direction, corresponding to the hexagonal axis of ST could not be identified by TEM, as all studied crystallites were encountered with this orientation almost parallel to the sample holder. Fortunately, this alignment of the flat lamellar crystals allowed determination of characteristic step heights related to this direction by AFM analysis.[47−49] For AFM, samples after removal of the mesodirecting template were studied. The analysis of the materials proved to be an extraordinary challenge, as the powders were difficult to fixate on the support. This problem was solved by pressing the samples into self-supporting wafers. A remarkable discovery was made: consistent step-heights of approximately 1.5 nm were observed, in full accordance with the height of the layers assumed to construct the hexagonal structures (Figure 4). Together with the TEM results, this observation led to the conclusion the newly assembled framework indeed was based on a hexagonal variant of HKUST-1 but with mesopore channels perpendicular to the 6-fold axis which reduced the symmetry from hexagonal to orthorhombic or monoclinic. Such a building principle also is in full accordance with the slab like morphology.

Combination of all results led to a construction of a new unit cell based on the ST structure (Figure 5). Comparison of the dimensions of the hexagonal layer resulted in excellent agreement of distances determined by TEM (3.6 and 2.1 nm) and the layer height of 1.5 nm observed by AFM. On the basis of this observation the symmetry of the ST structure was successively decreased to *P*2/*m* while keeping the all angles at 90°, due to the rigidity of the building units (Figure 5). In this setting, the positions of the Keggin ions allowed introduction of systematic porosity. In Figure 5, crystallographically different Keggin ions are marked in different colors. In the new cell with b = 3.1 nm, c = 2.1 nm, and a = 3.6 nm, the *ac* plane coincided with the original (001) plane, the new *ab* plane with (100) and the new *bc* plane with (120) of the ST model. Along the new c axis, now rows of Keggin ions with distances between the rows of 1.75 nm occur perpendicular to the step height of 1.5 nm. Systematic removal of parts of the framework every second row could result

dx.doi.org/10.1021/ja302089w | *J. Am. Chem. Soc.* 2012, 134, 10911−10919

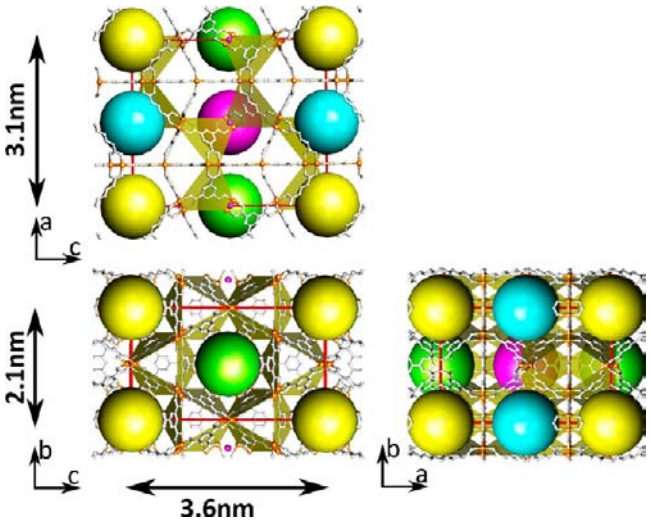

Figure 5. The ST model shows a metric which matches the dimensions observed by XRD, TEM and AFM. New structure based on symmetry reduced ST. Space group *P*2/*m* was chosen to allow introduction of systematic porosity as observed by TEM. Large spheres correspond to crystallographically diffferent positions of Keggin ions.

in the correct pore alignment and pore distance as determined by TEM. From a purely geometric argument, 2 different possibilities existed. Either only the central rows of Keggin could be removed (purple in Figure 5) or Keggin rows in the center and at the corner (purple and yellow) could be omitted resulting in a twice as high mesoporosity. Four arguments count against the latter scenario: (i) as seen from TEM in the highest magnification, the contrast did not change between steps along [001]. The bright and dark lines continue, even where according to slight changes of focus, a terrace on the *ac* plane ended. Removal of purple and yellow Keggin should lead to a switch in contrast between terraces. (ii) The removal of 50% of the framework as in the purple/yellow solution would lead to a much higher mesoporosity as observed by N_2 adsorption (vide infra); (iii) the ratio of organic BTC linkers and inorganic framework components would not match the chemical composition experimentally determined (vide infra); and (iv) in all probability, the framework would substantially loose stability. The new structure model of crystalline mesoporous COK-15 was constructed (Figure 6a). Partial removal of the framework led to partially exposed Cu-pairs per unit cell, coordinated by only 3 instead of 4 BTC linkers. It was assumed in the presence of water, these pairs most probably interact with water molecules and, to maintain a charge balanced net formula, hydroxide ions. The presence of the bridging hydroxyl group was confirmed by the FTIR spectra which display a broad band at 3495 cm^{-1} upon dehydration to 200 °C (Supporting Information Figure S3).[50]

To confirm the proposed model structure with the experimental XRD pattern, the corresponding pattern was simulated (Figure 6b). The positions of experimental reflections agreed satisfactorily with the simulated data and was strongly supported by the extensive evidence obtained by XRD, TEM, and AFM. Thus, it can be concluded the structure model correctly describes the structure of COK-15. The arrangement of the Keggin containing cages in this structure leads to a noteworthy shape of the mesopores. The straight channels along *b* give access to large side pockets in [101] and [$\bar{1}$01] direction. The size of these side pockets corresponds to the cavities of HKUST-1 and is accessible from the main straight channel via openings of 1.8 nm × 0.8 nm along [110] and 1.3 nm × 1.8 nm along [$\bar{1}$10]. This implies the mesopores widen along the diagonals of the *ac* planes up to 4.7 nm (Figure 6c). From the side pockets, guest molecules have access to cages occupied by Keggin ions via openings of 1.8 nm × 1.8 nm. Strong support for this structure model was obtained by direct simulation of the crystallographic orientation of the mesopores assigned through a TEM diffraction pattern. The simulated structure model matches perfectly when superimposed onto a high-magnification TEM image of a crystal, demonstrating the pore repetition (Figure 6d).

The chemical composition according to the proposed crystallographic model corresponds to $[Cu_{46}(C_9H_3O_6)_{24}(OH)_{12}]$ $(PW_{12}O_{40})_3$. This theoretical composition was in agreement with the chemical analysis of anhydrous COK-15 (in parentheses): W 39.6 wt % (39.6); P 0.56 wt % (0.56); Cu 17.5 wt % (16.2); C 15.5 wt % (17.4). The COK-15 compositional formula of $[Cu_{46}(C_9H_3O_6)_{24}(OH)_{12}]$ $(PW_{12}O_{40})_3$ carries a net negative charge and needs charge balancing. CTA cation adsorbed in the pores qualifies for this and the presence of residual CTA after leaching was confirmed by FTIR (Supporting Information Figure S3). The carbon excess found in the chemical analysis (17.4 versus 15.5 wt %) corresponds to ca. 1.4 CTA cations per formula, close to one CTA strictly needed for charge compensation. All this leads to an idealized chemical formula of $(CTA)_1[Cu_{46}(C_9H_3O_6)_{24}(OH)_{12}]$ $(PW_{12}O_{40})_3$.

As-synthesized sample contains larger amounts of CTAB. About 20 wt % of as-synthesized COK-15 consisted of CTAB that could be extracted via Soxhlet. However, unlike ordered mesoporous silica materials in COK-15 synthesis, the involvement of supramolecular CTAB micelles in the generation of mesopores within the material is questionable. The observed content of CTAB in as synthesized material would correspond to approximately 13 molecules per unit cell, which is too large a number to be all accommodated within the mesopores. The corrugated shape of the mesopores seems imposed rather by charge compensation and coordination requirements of the copper dimers and Keggin ions. The observation that already small amounts of CTAB start to affect the morphology of the obtained crystallites indicates individual CTA ions can be incorporated to act as void fillers and charge compensation. The second observation that high concentrations of CTAB in the synthesis fully change the morphology to lamellar could be taken as indication the structure directing role of CTAB is 2-fold: inclusion of CTA in the pores changes pore topology toward mesoporous and externally present surfactant in solution facilitates the expression of flat, extended sheets. To verify this, syntheses with quaternary ammonium compounds with different alkyl chain length were performed. As the current model of the formation of COK-15 depends on the rearrangement of structural units derived from the HKUST-1, similar *d*-spacings should be expected independent of the length of the organic template, while in case of a micelle directed growth, the dimensions of the framework should change drastically. Preliminary attempts to use templates with varying chain length as template indeed revealed no significant effect on pore size and the PXRD patterns still showed the typical distances to be expected when the same building principle was followed. Closer investigations of these materials are currently performed (Supporting Information Figure S4).

The stability of COK-15 materials after elimination of CTAB was confirmed by XRD. The retention of intact HPW after the leaching process was confirmed by Fourier transform infrared spectroscopy (FTIR) and ^{31}P solid-state magic angle spinning

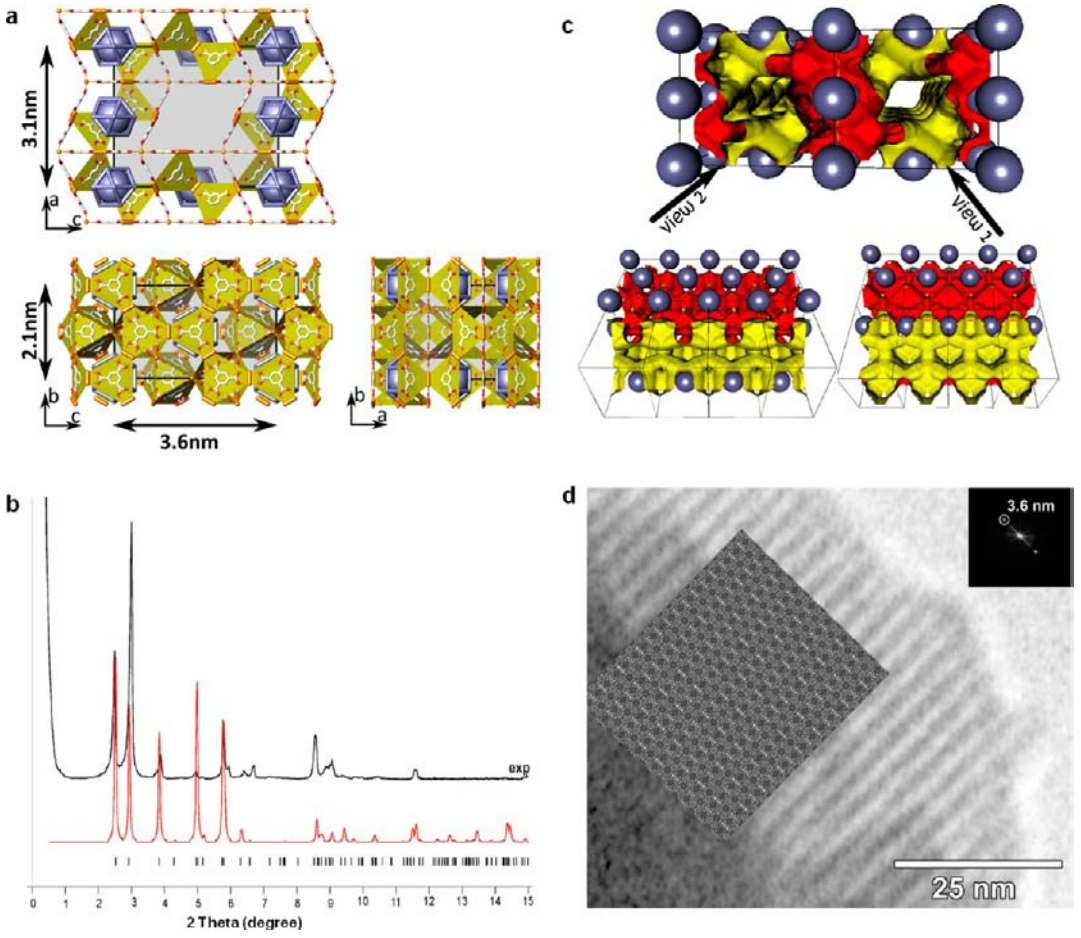

Figure 6. Proposed structure model of COK-15 by XRD and TEM simulation. (a) Proposed structure model of COK-15 shown along the *ac*, *bc*, and *ab* plane. Blue spheres indicate Keggin ions, yellow triangles BTC linkers, and orange rods Cu-pairs. Unit cell highlighted with black edges and gray faces. (b) Comparison of measured COK-15 (black) and simulated (red) XRD patterns. (c) Pore view of COK-15 obtained by rolling a sphere of 0.15 nm over the crystal structure. Top: view along the pore (b direction). Bottom: Views of pore after being sliced open. Framework was removed by diagonally cutting off half of the unit cell. (d) TEM image of COK-15 revealed the long axis of the mesoporous rods corresponded to the pore direction. Distance between pores was determined as 3.6 nm with a lattice spacing perpendicular to it of 2.1 nm determined from electron diffraction. Comparison of the crystallographic evidence resulted in assignment of the view direction as either [111] in a cubic or [001] in a hexagonal setting. On the right, a simulated image at crystal thickness t = 97 nm and defocus Δf = −115 nm is inserted into a high magnification image, clearly demonstrating the pore repetition.

nuclear magnetic resonance spectroscopy (MAS NMR) (Supporting Information Figure S5).[51] Leached COK-15 material was stable for at least two years upon storage in ambient air (Supporting Information Figure S6).

The porosity of COK-15 was probed using N_2 adsorption (Supporting Information Figure S7). The N_2 adsorption isotherm was characterized by a strong uptake at low relative pressure ascribed to microporosity. The presence of hysteresis between adsorption and desorption branches of the isotherm at higher relative pressures was attributed to mesoporosity. The shape of the hysteresis loop (H2 type) hints at the presence of "bottleneck" pores with larger cages accessible via smaller openings.[52] According to the Barret–Joyner–Halenda (BJH) method (Supporting Information Figure S7, inset), the diameter of the mesopores is about 5 nm as predicted by the model. COK-15 has a BET (Brunauer–Emmet–Teller) and Langmuir surface area of 100 and 130 $m^2\ g^{-1}$, respectively. These are moderate values compared to often 1 order of magnitude higher values attained by the most spacious MOFs in literature. Incorporation of heavy HPW ions representing ca. 55 wt % of COK-15 material is a reason, as well as the presence of residual CTA ions in the pores which could partially block the access to the pores, especially at the very low temperature at which N_2 porosimetry is performed. The adsorption of acetonitrile is convenient for probing the porosity of a MOF material at ambient temperature.[53] COK-15 sample was evacuated at 150 °C and exposed to acetonitrile vapor for 48 h at room temperature. The COK-15 structure model presents an estimated solvent accessible surface of 900 $m^2\ g^{-1}$ and a solvent-accessible pore volume of 5850 $Å^3$, which corresponds to 25% of the unit-cell volume (23 400 $Å^3$). The pore volume estimated from the acetonitrile adsorption capacity was 14.5 vol %, and close to the theoretical pore volume considering the presence of occluded CTA. Acetonitrile adsorption was reversible.

The catalytic performance of COK-15 was investigated using alcoholysis of styrene oxide as a model reaction under mild conditions. This ring-opening reaction of styrene oxide with methanol was performed at 40 °C. The 2-methoxy-2 phenylethanol reaction product is a valuable organic solvent and intermediate for pharmaceutical and chemical industries.[54] Epoxide ring methanolysis is catalyzed by strong acid or base catalysts, and is often suffering from low selectivity. Interestingly, COK-15 showed remarkable catalytic activity achieving 100% conversion of styrene oxide with 100% selectivity for 2-methoxy-

dx.doi.org/10.1021/ja302089w | J. Am. Chem. Soc. 2012, 134, 10911–10919

2 phenylethanol after 3 h (Supporting Information Figure S8a). Presumably coordinatively unsaturated copper dimers in the mesopore walls are the active sites.[55] Under similar reaction conditions, the microporous HKUST-1 HPW@$Cu_3(BTC)_2$ reference reached only 40% conversion. The use of HKUST-1 $Cu_3(BTC)_2$ reference as catalyst and reaction in absence of catalyst resulted in less than 2% conversion. This result suggests that the mesoporous feature of COK-15 efficiently reduced mass transport limitation of the reaction. Microporous HZSM-5 zeolite showed >98% conversion of styrene oxide after 1 h under similar reaction conditions, but poor selectivity (62%). To verify the heterogeneity of the catalyst, the suspended COK-15 catalyst was removed via centrifugation after 1 h. In the clear supernatant, no further product formation was observed upon heating (Supporting Information Figure S8b). This proved the true heterogeneous nature of the COK-15 catalyst. Moreover, the catalyst could be reused for at least 4 catalytic runs maintaining high catalytic activity (>90%) and selectivity to 2-methoxy-2 phenylethanol even without the need of any catalyst regeneration (Supporting Information Figure S8c).

CONCLUSIONS

In conclusion, we have shown the successful synthesis of the first MOF with crystalline repetitive motifs of long-range ordered monoclinic mesostructure separated by microstructured walls and its crystallization via a combined template and surfactant synthesis approach at room temperature. The concept of co-templation is proven by the obtained structure and could possibly be applied to other microporous MOFs. The new crystalline mesoporous MOF has substantially wide permanent mesopores demonstrating excellent catalytic activity and selectivity in methanolysis of styrene oxide under mild reaction conditions. Besides application in selective catalysis, the availability of a robust MOF with such wide mesopores could be useful for molecular separation, gas storage, and development of biomedical applications such as controlled release, drug delivery, detection and sensing of biological species, for example, small viruses, and multimodal bioimaging with simultaneous diagnosis and therapy functions.

ASSOCIATED CONTENT

Supporting Information

Cubic microporous structure of HPW@$Cu_3(BTC)_2$, characterization of COK-15 by TGA, FTIR, XRD, ^{31}P solid-state MAS NMR, N_2 adsorption, and catalytic testing. This material is available free of charge via the Internet at http://pubs.acs.org.

AUTHOR INFORMATION

Corresponding Author

Christine.Kirschhock@biw.kuleuven.be

Notes

The authors declare no competing financial interest.

ACKNOWLEDGMENTS

L.H.W., N.J., S.R.B., C.E.A.K. and J.A.M gratefully acknowledge financial supports from Flemish Government (Long-term structural funding-Methusalem) and the Belgium Government (IAP-PAI networking). C.W. and G.V.T. acknowledge support from the European Union under the Framework 7 program under a contract from an Integrated Infrastructure Initiative (Reference 262348 ESMI). S.T. gratefully acknowledges financial support from the Fund for Scientific Research Flanders (FWO). S. D. thanks the Fund of Scientific Research-Flanders (FWO) and the Belgian Federal Science Policy Office through IAP-6/27. W.V. is grateful to the Agency for Innovation by Science and Technology in Flanders (IWT). The authors thank Dr Alexander Aerts and Dr Elena Gobechiya for XRD measurements.

REFERENCES

(1) Férey, G. *Chem. Soc. Rev.* **2008**, *37*, 191.
(2) Yaghi, O. M.; O'Keeffe, M.; Ockwig, N. W.; Chae, H. K.; Eddaoudi, M.; Kim, J. *Nature* **2003**, *423*, 705.
(3) Corma, A.; García, H.; Llabrés I Xamena, F. X. *Chem. Rev.* **2010**, *110*, 4606.
(4) Hong, D. -Y.; Hwang, Y. K.; Serre, C.; Férey, G.; Chang, J. -S. *Adv. Funct. Mater.* **2009**, *19*, 1537.
(5) Chui, S. S. -Y.; Lo, S. M. -F.; Charmant, J. P. H.; Orpen, A. G.; Williams, I. D. *Science* **1999**, *283*, 1148.
(6) Hayashi, H.; Côté, A. P.; Furukawa, H.; O'Keeffe, M.; Yaghi, O. M. *Nat. Mater.* **2007**, *6*, 501.
(7) Beldon, P. J.; Fábián, L.; Stein, R. S.; Thirumurugan, A.; Cheetham, A. K.; Friščić, T. *Angew. Chem., Int. Ed.* **2010**, *49*, 9640.
(8) Wharmby, M. T.; Mowat, J. P. S.; Thompson, S. P.; Wright, P. A. *J. Am. Chem. Soc.* **2011**, *133*, 1266.
(9) Eddaoudi, M.; Kim, J.; Rosi, N.; Vodak, D.; Wachter, J.; O'Keeffe, M.; Yaghi, O. M. *Science* **2002**, *295*, 469.
(10) Rocca, J. D.; Liu, D.; Lin, W. *Acc. Chem. Res.* **2011**, *44*, 957.
(11) Horcajada, P.; Chalati, T.; Serre, C.; Gillet, B.; Sebrie, C.; Baati, T.; Eubank, J. F.; Heurtaux, D.; Clayette, P.; Kreuz, C.; Chang, J.-S.; Hwang, Y. K.; Marsaud, V.; Bories, P.-N.; Cynober, L.; Gil, S.; Férey, G.; Couvreur, P.; Gref, R. *Nat. Mater.* **2010**, *9*, 172.
(12) Gu, Z.-Y.; Chen, Y.-J.; Jiang, J.-Q.; Yam, X.-P. *Chem. Commun.* **2011**, *47*, 4787.
(13) Lykourinou, V.; Chen, Y.; Wang, X.-S.; Meng, L.; Hoang, T.; Ming, L.-J.; Musselman, R. L.; Ma, S. *J. Am. Chem. Soc.* **2011**, *133*, 10382.
(14) Férey, G.; Mellot-Draznieks, C.; Serre, C.; Millange, F.; Dutour, J.; Surblé, S.; Margiolaki, I. *Science* **2005**, *309*, 2040.
(15) Park, Y. K.; Choi, S. B.; Kim, H.; Kim, K.; Won, B.-H.; Choi, K.; Choi, J.-S.; Ahn, W.-S.; Won, N.; Kim, S.; Jung, D. H.; Choi, S.-H.; Kim, G.-H.; Cha, S.-S.; Jhon, Y. H.; Yang, J. K.; Kim, J. *Angew. Chem., Int. Ed.* **2007**, *46*, 8230.
(16) Klein, N.; Senkovska, I.; Gedrich, K.; Stoeck, U.; Henschel, A.; Mueller, U.; Kaskel, S. *Angew. Chem., Int. Ed.* **2009**, *48*, 9954.
(17) Wang, B.; Côté, A. P.; Furukawa, H.; O'Keeffe, M.; Yaghi, O. M. *Nature* **2008**, *453*, 207.
(18) Wang, X. -S.; Ma, S.; Sun, D.; Parkin, S.; Zhou, H.-C. *J. Am. Chem. Soc.* **2006**, *128*, 16474.
(19) Horcajada, P.; Surblé, S.; Serre, C.; Hong, D.-Y.; Seo, Y.-K.; Chang, J.-S.; Grenèche, J.-M.; Margiolaki, I.; Férey, G. *Chem. Commun.* **2007**, *27*, 2820.
(20) Zhao, Y.; Zhang, J.; Han, B.; Song, J.; Li, J.; Wang, Q. *Angew. Chem., Int. Ed.* **2011**, *50*, 636.
(21) Koh, K.; Wong-Foy, A. G.; Matzger, A. J. *Angew. Chem., Int. Ed.* **2008**, *47*, 677.
(22) Yaghi, O. M. *Nat. Mater.* **2007**, *6*, 92.
(23) Shekhah, O.; Wang, H.; Paradinas, M.; Ocal, C.; Schüpbach, B.; Terfort, A.; Zacher, D.; Fischer, R. A.; Wöll., C. *Nat. Mater.* **2009**, *8*, 481.
(24) Choi, M.; Na, K.; Kim, J.; Sakamoto, Y.; Terasaki, O.; Ryoo, R. *Nature* **2009**, *461*, 246.
(25) Na, K.; Jo, C.; Kim, J.; Cho, K.; Jung, J.; Seo, K.; Messinger, R. J.; Chmelka, B. F.; Ryoo, R. *Science* **2011**, *333*, 328.
(26) Qiu, L. -G.; Xu, T.; Li, Z.-Q.; Wang, W.; Wu, Y.; Jiang, X.; Tian, X.-Y.; Zhang, L.-D. *Angew. Chem., Int. Ed.* **2008**, *47*, 9487.
(27) Sun, L.-B.; Li, J.-R.; Park, J.; Zhou, H.-C. *J. Am. Chem. Soc.* **2012**, *134*, 126.
(28) Roy, X.; MacLachlan., M. J. *Chem.—Eur. J.* **2009**, *15*, 6552.
(29) Hundal, G.; Hwang, Y. K.; Chang, J. -S. *Polyhedron* **2009**, *28*, 2450.
(30) Sun, C. -Y.; Liu, S.-X.; Liang, D.-D.; Shao, K.-Z.; Ren, Y.-H.; Su, Z.-M. *J. Am. Chem. Soc.* **2009**, *131*, 1883.

(31) Canioni, R.; Roch-Marchal, C.; Sécheresse, F.; Horcajada, P.; Serre, C.; Hardi-Dan, M.; Férey, G.; Grenèche, J.-M.; Lefebvre, F.; Chang, J.-S.; Hwang, Y.-K.; Lebedev, O.; Turner, S; Van Tendeloo, G. *J. Mater. Chem.* **2011**, *21*, 1226.
(32) Juan-Alcañiz, J.; Goesten, M.; Martinez-Joaristi, A.; Stavitski, E.; Petukhov, A. V.; Gascon, J.; Kapteijn, F. *Chem. Commun.* **2011**, *47*, 8578.
(33) Juan-Alcañiz, J.; Ramos-Fernandez, E. V.; Lafont, U.; Gascon, J.; Kapteijn, F. *J. Catal.* **2010**, *269*, 229.
(34) Li, S.; Zhang, D.; Guo, Y.; Ma, P.; Zhao, J.; Wang, J.; Niu, J. *Eur. J. Inorg. Chem.* **2011**, *2011*, 5397.
(35) Yu, F.; Zheng, P.-Q.; Long, Y.-X.; Ren, Y.-P.; Kong, X.-J.; Long, L.-S.; Yuan, Y.-Z.; Huang, R.-B.; Zheng, L.-S. *Eur. J. Inorg. Chem.* **2010**, *2010*, 4526.
(36) Maksimchuk, N. V.; Kovalenko, K. A.; Arzumanov, S. S.; Chesalov, Y. A.; Melgunov, M. S.; Stepanov, A. G.; Fedin, V. P.; Kholdeeva, O. A. *Inorg. Chem.* **2010**, *49*, 2920.
(37) Zhang, Y.; Degirmenci, V.; Li, C.; Hensen, E. J. M. *ChemSusChem* **2011**, *4*, 59.
(38) Bajpe, S. R.; Kirschhock, C. E. A.; Aerts, A.; Breynaert, E.; Absillis, G.; Parac-Vogt, T. N.; Giebeler, L.; Martens, J. A. *Chem.—Eur. J.* **2010**, *16*, 3926.
(39) Mustafa, D.; Breynaert, E.; Bajpe, S. R.; Martens, J. A.; Kirschhock, C. E. A. *Chem. Commun.* **2011**, *47*, 8037.
(40) Wee, L. H.; Janssens, N.; Bajpe, S. R.; Kirschhock, C. E. A.; Martens, J. A. *Catal. Today* **2011**, *171*, 275.
(41) Song, J.; Luo, Z.; Britt, D. K.; Furukawa, H.; Yaghi, O. M.; Hardcastle, K. I.; Hill, C. L. *J. Am. Chem. Soc.* **2011**, *133*, 16839.
(42) Kresge, C. T.; Leonowicz, M. E.; Roth, W. J.; Vartuli, J. C.; Beck, J. S. *Nature* **1992**, *359*, 710.
(43) Zhao, D.; Feng, J.; Huo, Q.; Melosh, N.; Fredrickson, G. H.; Chmelka, B. F.; Stucky, G. D. *Science* **1998**, *279*, 548.
(44) Jammaer, J.; van Erp, T. S.; Aerts, A.; Kirschhock, C. E. A.; Martens, J. A. *J. Am. Chem. Soc.* **2011**, *133*, 13737.
(45) Eddaoudi, M. *Nature* **2007**, *6*, 718.
(46) Turner, S.; Lebedev, O. I.; Schröder, F.; Esken, D.; Fischer, R. A.; Van Tendeloo, G. *Chem. Mater.* **2008**, *20*, 5622.
(47) Shoaee, M.; Anderson, M. W.; Attfield, M. P. *Angew. Chem., Int. Ed.* **2008**, *47*, 8525.
(48) John, N. S.; Scherb, C.; Shöâeè, M.; Anderson, M. W.; Attfield, M. P.; Bein, T. *Chem. Commun.* **2009**, 6294.
(49) Szelagowska-Kunstman, K.; Cyganik, P.; Goryl, M.; Zacher, D.; Puterova, Z.; Fischer, R. A.; Szymonski, M. *J. Am. Chem. Soc.* **2008**, *130*, 14446.
(50) Youngme, S.; Phatchimkun, J.; Wannarit, N.; Chaichit, N.; Meejoo, S.; van Albada, G. A.; Reedijk, J. *Polyhedra* **2008**, *27*, 304.
(51) Wee, L. H.; Bajpe, S. R.; Janssens, N.; Hermans, I.; Houthoofd, K.; Kirschhock, C. E. A.; Martens, J. A. *Chem. Commun.* **2010**, *46*, 8186.
(52) Sing, K. S. W.; Everett, D. H.; Haul, R. A. W.; Moscou, L.; Pierotti, R. A.; Rouquerol, J.; Siemieniewska, T. *Pure Appl. Chem.* **1985**, *57*, 603.
(53) Streb, C.; Ritchie, C.; Long, D.-L.; Kögerler, P.; Cronin, L. *Angew. Chem., Int. Ed.* **2007**, *46*, 7579.
(54) Tokunaga, M.; Larrow, J. F.; Kakiuchi, F.; Jacobsen, E. N. *Science* **1997**, *277*, 936.
(55) Janssens, N.; Wee, L. H.; Bajpe, S.; Breynaert, E.; Kirschhock, C. E. A.; Martens, J. A. *Chem. Sci.* **2012**, *3*, 1047.